Light scattering properties of a solar panel including wavelength and polarization dependencies in the visible spectrum

Joe Kurtz[*]
University of New South Wales – Canberra, Australia
Andrew Jolley
Western Sydney University, Australia

Scott Tyo
University of New South Wales – Canberra, Australia

ABSTRACT

A polarimetric scatterometer was designed and constructed at UNSW-Canberra's Advanced Sensing Laboratory to enable the production of spectrally-resolved material bi-directional reflectance distribution functions (BRDFs). The capability to characterise the polarization properties of light scattered from those materials yields a complete Mueller matrix from which a polarimetric BRDF (*p*BRDF) can be determined. In this study, the Mueller matrix of a triple junction solar cell sample was characterized to demonstrate the polarimetric measurement capabilities of the scatterometer as a function of wavelength.

1. INTRODUCTION

The Polarimetric Scatterometer, Fig. 1, consists of multiple motorized stages configured to arrange a sample, a light source, and detector/imager such that the scattering of light (via transmission, refraction, or reflection) from a sample at nearly any set of angles can be measured. When the source and detector are fitted with appropriate polarizing optical elements, the instrument becomes a scattered-light polarimeter. The light source is a variable-wavelength monochromator which adds spectrally-resolved measurement capability to the instrument. The light source, detector/imager, any rotatable optics, and all motorized stages (sample orientation) are controlled by a single laptop computer which can also record the data.

Samples of interest include typical spacecraft materials, the scattering properties of which are required to model and identify spacecraft or debris for space situational awareness (SSA) purposes [1]. Using the Scatterometer, the reflectance of a sample material can be measured (as a function of wavelength) over the incident and observation angle for a wide range of sample orientations resulting in a nearly complete bi-directional reflectance distribution function (BRDF) although such an exhaustive study was not done for this paper.

With a comprehensive library of spacecraft material BRDFs, observed optical signals from orbiting objects could be compared to known optical properties to identify the surface materials of those objects. NASA's Optical Measurements Center (OMC), for example, has been working for some time on the development of a spacecraft materials BRDF database that could be used in conjunction with observations of orbiting objects to improve size estimation calculations [2]. The Astronomical Institute at the University of Bern (AIUB) has accumulated a large database of spacecraft lightcurves with the goal of better characterising the space debris environment [3], including identifying high-area to mass ratio debris by comparison to laboratory acquired spectral data [4]. The OMC uses Johnson/Bessel photometric filters to separate the reflected light into broad wavelength bands. Others have acquired high spectral resolution laboratory reflectance data of spacecraft materials, but the range of orientation angles has often been limited to near the specular reflection in order to maximise the signal received by the detector [5].

Polarimetric measurements can yield a complete Mueller matrix useful for predicting the polarization properties of light scattered from these materials and from which a polarimetric BRDF (*p*BRDF) can be determined. The authors

[*]j.kurtz@unsw.edu.au

are not aware of any efforts to produce a spacecraft materials database that comprises both high spectral resolution and polarimetric information with high spatial resolution across the entire hemispherical range of illumination / observation geometries. Combining all of these aspects would provide the best chance of identifying surface material types with confidence.

This study investigates the specular reflection properties of a fragment of a solar cell over a limited angular range as a function of wavelength to demonstrate the Scatterometer's polarimetric measurement capabilities.

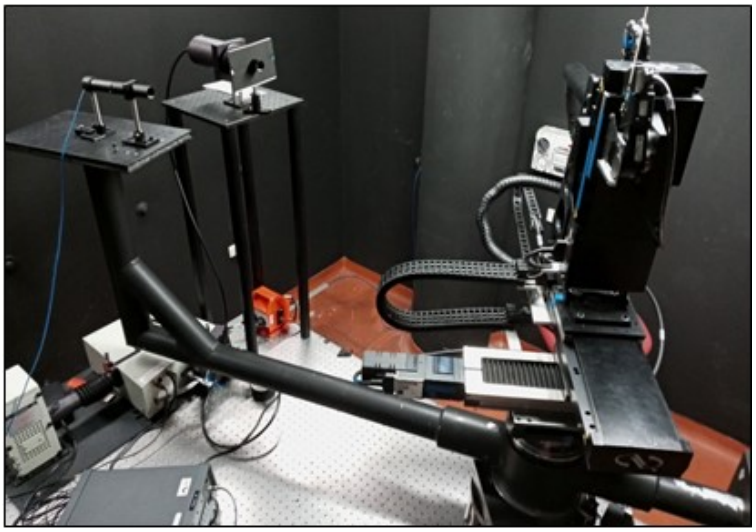

Fig. 1: The "Polarimetric Scatterometer" of the Advanced Sensing Laboratory at the University of New South Wales – Canberra was used in this study.

2. BACKGROUND

The basic polarimetric equation describing the measurements is easily expressed in terms of four-element Stokes vectors describing the polarization state of light as

$$\mathbf{S} = [S_0\ S_1\ S_2\ S_3]^T$$

where the elements are in terms of the intensities:

$$S_0 = I = \text{total flux;}$$

$$S_1 = I_0 - I_{90} = 0^\circ, 90^\circ \text{ horizontal, vertical polarization difference;}$$

$$S_2 = I_{45} - I_{135} = 45^\circ, 135^\circ \text{ diagonal polarization difference;}$$

$$S_3 = I_{Right} - I_{Left} = \text{right, left circular polarization difference;}$$

where the subscripts refer to polarizations as measured by ideal polarizers in front of a detector as noted in [6].

Describing the incoming light with the Stokes vector, $\mathbf{S}_{in}$, and the scattered light with $_{scat}$, a 4×4 Mueller matrix, $\underline{\underline{\mathbf{M}}}$, describes the interaction of the sample with the incoming light to produce the polarization state of the scattered light:

$$\mathbf{S}_{scat} = \underline{\underline{\mathbf{M}}}\, \mathbf{S}_{in}.$$

The term 'scattered light' here refers to any light reflected or transmitted by the sample into the direction of the detector. To characterize the polarization of the scattered light, it is passed through one or more optical elements, such as a linear polarizer, before reaching a detector. This analyzer can be also described by a 4×4 Mueller matrix. However, the detection of the light after the analyzer is purely an intensity measurement and does not reveal a complete stokes

vector. Therefore, only the top row of the analyzer's Mueller matrix need be considered, and this row is known as the analyzer vector. Using several different analyzer configurations can result in a sufficient number of measurements to characterize the stokes vector of the scattered light. The equation describing this situation for each analyzer $\mathbf{A}_i$ is:

$$I_i = \mathbf{A}_i \underline{\underline{\mathbf{M}}} \mathbf{S}_{in}.$$

An unpolarized light source must pass through assorted sets of optical elements in order to generate a sufficient variety of polarization states. Each unique polarization state, j, so generated has a corresponding stokes vector, usually denoted W_j, referred to as a generator vector. Substituting $\mathbf{W}_j$ for $\mathbf{S}_{in}$, for each combination of a generator, j, and an analyzer, i, results in an intensity measurement, I_{ij}, and the above equation can be re-expressed in terms of the generator and analyzer vectors:

$$I_{i,j} = \mathbf{A}_i \underline{\underline{\mathbf{M}}} \mathbf{W}_j$$

If we have selected n different analyzer vectors and m different generator vectors, the measured intensities can be expressed as an $n \times m$ matrix, $\underline{I}$, which is the product of the $n \times 4$ matrix of analyzer vectors, $\underline{\underline{\mathbf{A}}}$, the 4×4 matrix, $\underline{\underline{\mathbf{M}}}$, and a $4 \times m$ matrix of generator vectors, $\underline{\underline{\mathbf{W}}}$:

$$\underline{I} = \underline{\underline{\mathbf{A}}}\,\underline{\underline{\mathbf{M}}}\,\underline{\underline{\mathbf{W}}}. \tag{1}$$

By measuring the intensities, $\underline{I}$, Eq. (1) becomes the basis for the experimental determination of the unknown, $\underline{\underline{\mathbf{M}}}$, once the generator and analyzer vectors are known [7].

3. EXPERIMENT

The optical setup is depicted schematically in Fig. 2. The half-wave retarder (HWR) and the quarter-wave retarder (QWR) were mounted on motorized stages that allowed the retarder fast axis of each to be rotated azimuthally around the optical beam axis. The LP conditioned the wavelength-selectable light source to be linearly polarized with the polarization axis set at horizontal (parallel) to the scattering plane which was considered the azimuthal "0 degrees". The HWR was used to change the linear polarization angle of the light while the QWR was used to create right- and left-circular polarization. Aligning either retarder's fast axis with the polarization axis of the LP would nullify its effect on the beam's polarization. The combinations of azimuthal angles for (HWR, QWR) elements used in the measurements were approximately (in degrees): (0,0), (22.5,0), (45,0), (67.5,0), (-45,0), (+45,0) which would ideally generate six states representing the modulation of each of the Stokes elements (S_1 to S_3) separately. This represents the "optimum" 6-measurement configuration for a stokes vector polarimeter and the optimum 36-measurement configuration for a Mueller matrix polarimeter [8]. Both optical elements were specified by the manufacturer to have their rated retardance at 670 nm wavelength and vary by 10% or less between 600 and 740 nm. Calibration measurements found them effective down to $\sim$ 550 nm although measurements down to 450 nm were attempted.

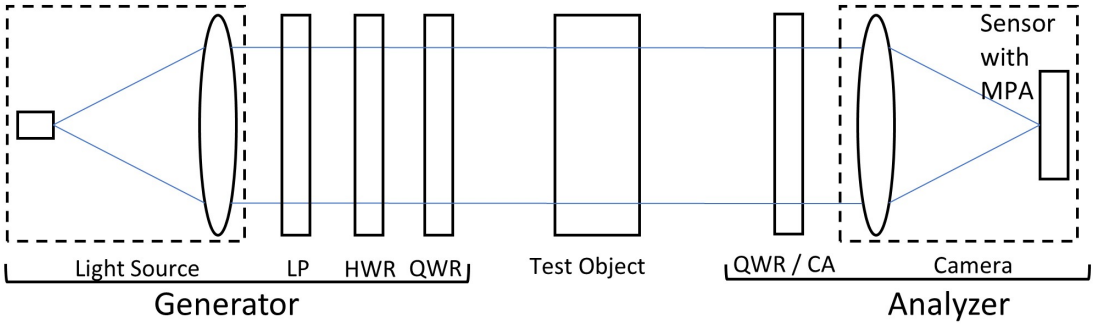

Fig. 2: The optical schematic: LP = Linear polarizer; HWR = Half-wave retarder; QWR = Quarter-wave retarder; CA = Clear aperture; MPA = Micro-polarizer array. The HWR and QWR of the Generator were mounted on azimuthally-rotatable stages. The QWR of the Analyzer could be moved out of the beam path in favor of a clear aperture. The test object could be measured either in transmission or reflection.

3.1 Calibration

This study made use of the Eigenvalue Calibration Method (ECM) as described in [9] and [10]. This method mathematically deduces the generator and analyzer states by using the measurements of a limited number of reference objects whose Mueller matrix elements are known. In brief and following [10], this method uses Eq. (1) as written for each reference object, k:

$$\underline{\underline{I}}_k = \underline{\underline{\mathbf{A}}}\,\underline{\underline{\mathbf{M}}}_k\,\underline{\underline{\mathbf{W}}} \tag{2}$$

If one of the reference objects is air, then $\underline{\underline{\mathbf{M}}}_{air}$ is the identity matrix and $\underline{\underline{I}}_{air} = \underline{\underline{\mathbf{A}}}\,\underline{\underline{\mathbf{W}}}$. One can then define a matrix $\underline{\underline{\mathbf{C}}}_k$ for each of the other reference objects as:

$$\underline{\underline{\mathbf{C}}}_k \equiv \underline{\underline{I}}_{air}^{-1}\underline{\underline{I}}_k = \left(\underline{\underline{\mathbf{A}}}\,\underline{\underline{\mathbf{W}}}\right)^{-1}\underline{\underline{\mathbf{A}}}\,\underline{\underline{\mathbf{M}}}_k\,\underline{\underline{\mathbf{W}}},$$

so that

$$\underline{\underline{\mathbf{C}}}_k = \underline{\underline{\mathbf{W}}}^{-1}\underline{\underline{\mathbf{M}}}_k\underline{\underline{\mathbf{W}}}.$$

Multiplying from the left by $\underline{\underline{\mathbf{W}}}$ yields

$$\underline{\underline{\mathbf{W}}}\,\underline{\underline{\mathbf{C}}}_k - \underline{\underline{\mathbf{M}}}_k\,\underline{\underline{\mathbf{W}}} = 0. \tag{3}$$

Defining the column-stacking operator, **vec**, as the operator that transforms a $n \times m$ matrix to a column vector of $n*m$ elements by copying column by column, and using the identity $\mathbf{vec}(\underline{\underline{\mathbf{JKF}}}) = (\underline{\underline{\mathbf{F}}}^T \otimes \underline{\underline{\mathbf{J}}})\mathbf{vec}(\underline{\underline{\mathbf{K}}})$ where $\otimes$ denotes the Kronecker product, Eq. (3) can then be rewritten as

$$\left(\underline{\underline{\mathbf{I}}}\otimes\underline{\underline{\mathbf{M}}}_k - \underline{\underline{\mathbf{C}}}_k^T \otimes \underline{\underline{\mathbf{I}}}\right)\mathbf{vec}\left(\underline{\underline{\mathbf{W}}}\right) = 0,$$

or

$$\underline{\underline{\mathbf{H}}}_k\,\mathbf{vec}\left(\underline{\underline{\mathbf{W}}}\right) = 0, \tag{4}$$

where $\underline{\underline{\mathbf{H}}}_k \equiv \left(\underline{\underline{\mathbf{I}}}\otimes\underline{\underline{\mathbf{M}}}_k - \underline{\underline{\mathbf{C}}}_k^T \otimes \underline{\underline{\mathbf{I}}}\right)$, and $\underline{\underline{\mathbf{I}}}$ is the identity matrix. Using n reference objects, an expression equivalent to (4) is:

$$\underline{\underline{\mathbf{L}}}\,\mathbf{vec}(\underline{\underline{\mathbf{W}}}) = 0 \tag{5}$$

where

$$\underline{\underline{\mathbf{L}}} \equiv \sum_{k=1}^{n} \underline{\underline{\mathbf{H}}}_k^T\underline{\underline{\mathbf{H}}}_k$$

and is guaranteed to be Hermitian. The desired solution, $\mathbf{vec}(W)$, is the eigenvector corresponding to the null eigenvalue of $\underline{\underline{\mathbf{L}}}$. If the number of generator/analyzer combinations is more than required, Eq. 5 is an overdetermined system and can by solved by the utilizing singular value decomposition to determine the eigenvalues and eigenvectors of $\underline{\underline{\mathbf{L}}}$ in the least squares sense.

In general, a zero eigenvalue may not be produced exactly, but the smallest eigenvalue indicates the best approximation of the solution, $\underline{\underline{\mathbf{W}}}$. Since the matrices $\underline{\underline{\mathbf{M}}}_k$ are theoretically generated, the parameters used (such as the polarization angle and diattenuation of a reference polarizer) can be varied by small amounts until the smallest eigenvalue of $\underline{\underline{\mathbf{L}}}$ is as close to zero as possible. Thus, these experimental parameters do not have to be known precisely during experimental set up but can be refined as a part of the calibration process in the search for the smallest eigenvalue of $\underline{\underline{\mathbf{L}}}$.

To produce only a single null eigenvalue, this calibration scheme requires that the generator be capable of producing (repeatably) a complete set of states that span the space of the Stokes vectors and that the analyzer likewise be capable of measuring this span. Success is indicated by the proximity to zero of the smallest eigenvalue of $\underline{\underline{\mathbf{L}}}$ and the quality of the corresponding generator vectors. The Appendix lists the actual generator vectors achieved for each wavelength and the corresponding eigenvalue. Analyzer vectors were deduced from $\underline{\underline{\mathbf{W}}}$ using the results of the measurements of air:

$$\underline{\underline{\mathbf{A}}} = \underline{\underline{I}}_{air}\underline{\underline{\mathbf{W}}}^{-1}.$$

The reference objects used for this calibration consisted of (1) air; (2) a beamsplitter cube used as a polarizer in transmission and set at three azimuthal angles with respect to the generator's LP (i.e., 0, ±45°); and (3) a quarter-wave

retarder specified as such for wavelengths between 630 and 835 nm by the manufacturer and set at approximately 45° with respect to the generator's LP. All reference object measurements were done in transmission.

As mentioned above, the parameters of the reference objects were subject to adjustment when searching for the minimum eigenvalues. These parameter were 1) the three azimuthal polarization angles and the diattenuation of the polarizing beamsplitter, and 2) the angle of the fast axis and retardance of the quarter-wave retarder, the latter being a function of wavelength.

The analyzer consisted of a QWR and a Lucid 5-megapixel camera using a 2448×2048-pixel 2D detector array with an integrated micro-polarizer array (MPA). The MPA/sensor combination measured the intensity of the incoming light at 0-, 45-, 90-, and 135-degree linear polarization (Fig. 3) with respect to the generator LP axis. The fast axis of the QWR was set at an azimuthal angle of approximately 45 degrees with respect to the generator LP and was alternately placed in and out of the beam for a total of eight analyzer vectors for each generator state. Note: The exact fast-axis angle and retardance of the analyzer QWR can be calculated from the calibration results, $\underline{\underline{\mathbf{A}}}$, if required.

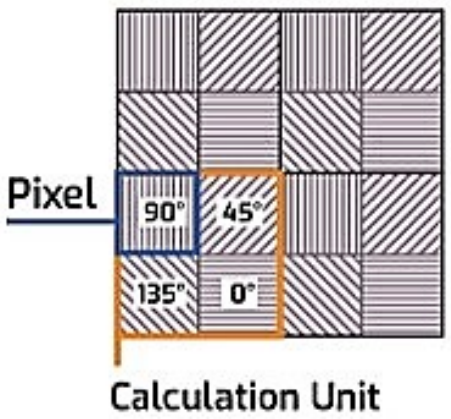

Fig. 3: Micro-polarizer array (MPA) integrated with sensor as a 2×2 calculational unit ('super-pixel') for concurrent measurement of four linear polarizations albeit with degraded spatial resolution.

Camera images were captured using acquisition software in MatLab. The imaged area of the sensor that was captured was 52×50 pixels. Saved image data was the average of 25 captured images of 8-bit intensity resolution. Exposure time and camera gain were adjusted to provide optimum signal without saturation. Separate measurements were taken of various gain and exposure-time settings under identical illumination conditions for each wavelength so that relative intensities between calibration, mirror, and sample measurements could be compared as the two parameters were necessarily varied for different conditions.

3.2 Mirror and Sample measurements

The sample studied here was a fragment of a SpectroLab Triple Junction solar cell of the type commonly used in CubeSat construction and previously studied by Jolley, et al, in [11]. Fig. 4 is a photo of the fragment as mounted in the Scatterometer. To keep it as flat as possible, it is adhered to the back face of a protected-silver first-surface mirror, the reflectance of which was also measured by flipping the mirror in the sample holder. The captured images from both the mirror and the sample are shown in Fig. 5 and demonstrate that the solar cell sample (bottom two images) was not reflecting as a flat surface as the image is distorted compared to that as seen through the mirror (top). The effect of this distortion could be a bias in the data resulting in a lower reflectance measurement than may be had from a more pristine sample.

The red rectangles in Fig. 5 indicate the four super-pixels that were used as the region of interest (ROI) in this study. After subtraction of a dark image (i.e. light source blocked), the four polarization data of each super-pixel were averaged together to derive the response at the four polarization states (0, 45, 90, 135) for each saved image. These values were then normalized to a common gain-exposure time setting so that intensities between calibration, mirror, and sample measurements would be relative to a common intensity scale.

Fig. 4: The SpectroLab solar cell fragment used in the measurements shown in the 'vertical' orientation. Measurements were done in two orientations: one as shown, and one horizontal (rotated 90°).

4. DATA ANALYSIS

Equation (1) (repeated here) is the equation relating generator vectors, $\underline{\underline{\mathbf{W}}}$, and the analyzer vectors, $\underline{\underline{\mathbf{A}}}$, to the intensity measurements of the ROI, $\underline{\underline{I}}$:

$$\underline{\underline{I}} = \underline{\underline{\mathbf{A}}}\,\underline{\underline{\mathbf{M}}}\,\underline{\underline{\mathbf{W}}}.$$

Multiplying by the inverse of $\underline{\underline{\mathbf{A}}}$ from the left and by the inverse of $\underline{\underline{\mathbf{W}}}$ from the right results in an expression for the Muller matrix, $\underline{\underline{\mathbf{M}}}$:

$$\underline{\underline{\mathbf{M}}} = \underline{\underline{\mathbf{A}}}^{-1}\,\underline{\underline{I}}\,\underline{\underline{\mathbf{W}}}^{-1} \tag{6}$$

The inversion of each matrix was accomplished by using the pseudo-inverse resulting from the singular-value decomposition (SVD) method while ignoring the singular values near zero.

It is of interest to characterize the physical properties of diattenuation, retardation, and depolarization that arise from the measured Mueller matrix, $\underline{\underline{\mathbf{M}}}$, of a material under study. A commonly used characterization of the depolarization property is the Depolarization Index [12] defined as:

$$P_D = \left(\frac{\sum_{i,j} \underline{\underline{\mathbf{M}}}_{i,j}^2 - \underline{\underline{\mathbf{M}}}_{0,0}^2}{3\underline{\underline{\mathbf{M}}}_{0,0}^2} \right)^{\frac{1}{2}}. \tag{7}$$

P_D varies from 0 for a completely depolarizing medium to 1 for a perfectly non-depolarizing medium.

Further processing of the Mueller matrices was performed using the polar decomposition method of [13] wherein a Mueller matrix is decomposed into a product of three Mueller matrices:

$$\underline{\underline{\mathbf{M}}} = \underline{\underline{\mathbf{M}}}_{\Delta}\underline{\underline{\mathbf{M}}}_{R}\underline{\underline{\mathbf{M}}}_{D}$$

where $\underline{\underline{\mathbf{M}}}_{D}$ is the Mueller matrix of a pure diattenuator, $\underline{\underline{\mathbf{M}}}_{R}$ is that of a pure retarder, and $\underline{\underline{\mathbf{M}}}_{\Delta}$ is that of a depolarizer. After using that method for the decomposition of $\underline{\underline{\mathbf{M}}}$, the diattenuation of $\underline{\underline{\mathbf{M}}}_{D}$ and the retardance of $\underline{\underline{\mathbf{M}}}_{R}$ can be calculated as

$$D = \sum_{k=1}^{3} \left(\underline{\underline{\mathbf{M}}}_{D} \right)_{0,k} \tag{8}$$

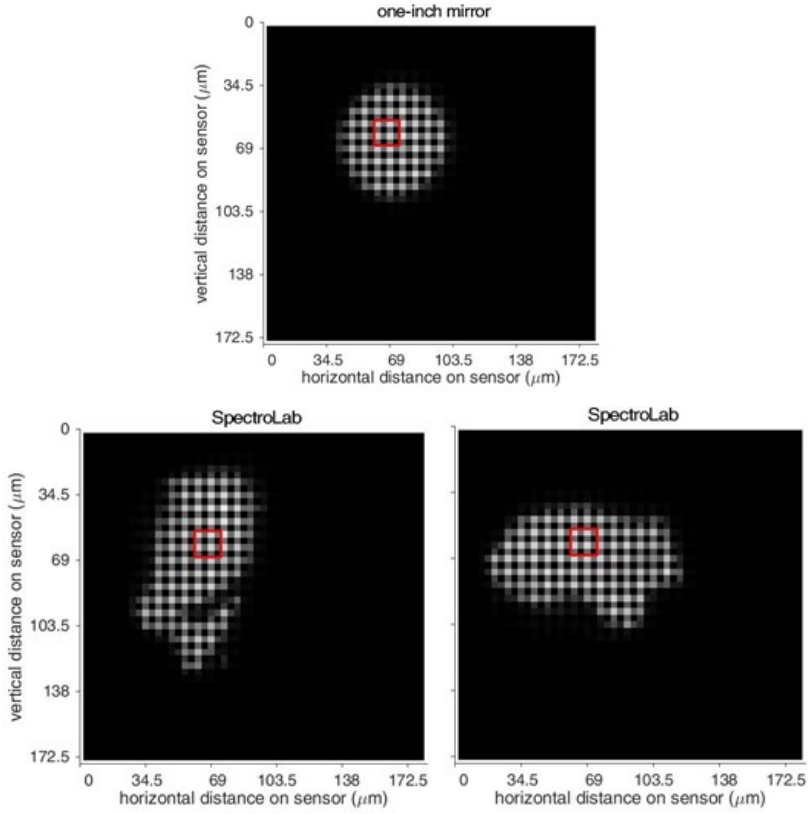

Fig. 5: Images captured by the camera for the flat mirror (top) and the SpectroLab fragment (bottom: vertical right, horizontal left). The SpectroLab sample distorted the image compared to the flat mirror. The red rectangle indicates the four super-pixels that were averaged in the data analysis to derive the response. The checkerboard pattern demonstrates the pixel-by-pixel polarization sensitivity of the camera when illuminated with linearly polarized light (horizontal in these photos).

and

$$R = \frac{1}{2\pi} \arccos\left(\frac{\mathrm{tr}(\underline{\underline{\mathbf{M}}}_R)}{2} - 1\right), \tag{9}$$

respectively, where the factor of 2π used in the latter expression converts radians to waves.

5. RESULTS AND DISCUSSION

Equation (10) [14] is the theoretical Mueller matrix for an isotropic surface from which light has been obliquely reflected expressed using the usual ellipsometric parameters, ψ and Δ, and taking into account the change of sign of the S_2 and S_3 Stokes components upon reflection [6]. It is equivalent to a partial linear polarizer at 90 degrees (with respect to the scattering plane) with relative amplitude attenuation $(\tau_{min}/\tau_{max})^{\frac{1}{2}} = (\tau_p/\tau_s)^{\frac{1}{2}} \equiv \tan\,\psi$; followed by a linear retarder of retardance Δ with fast axis at 0 degrees with respect to the scattering plane (or -Δ with fast axis at 90 degrees).

$$\underline{\underline{\mathbf{M}}} = \frac{\tau_{max} + \tau_{min}}{2} \begin{pmatrix} 1 & -\cos 2\psi & 0 & 0 \\ -\cos 2\psi & 1 & 0 & 0 \\ 0 & 0 & \sin 2\psi\,\cos\Delta & \sin 2\psi\,\sin\Delta \\ 0 & 0 & -\sin 2\psi\,\sin\Delta & \sin 2\psi\,\cos\Delta \end{pmatrix} \tag{10}$$

Table 1 refers to a protected silver first-surface mirror and Table 2 refers to the SpectroLab solar cell sample each being measured at two azimuthal orientations (parallel and perpendicular) to the scattering plane. Measurements were

Table 1: Typical Mueller matrix results for the mirror at specular reflection half-angle of 15 degrees.
wavelength (nm): 600.0 Sample: One-inch mirror Orientation: horizontal.

$$0.7979 \cdot \begin{pmatrix} 1.0000 & 0.0108 & 0.0041 & -0.0068 \\ 0.0204 & 0.9952 & 0.0049 & 0.0015 \\ 0.0104 & 0.0040 & -1.0048 & 0.0098 \\ -0.0023 & -0.0054 & -0.0001 & -1.0068 \end{pmatrix}$$

wavelength (nm): 600.0 Sample: One-inch mirror Orientation: vertical.

$$0.7975 \cdot \begin{pmatrix} 1.0000 & 0.0105 & 0.0033 & -0.0075 \\ 0.0221 & 0.9969 & 0.0034 & 0.0046 \\ 0.0088 & 0.0053 & -1.0031 & 0.0099 \\ -0.0013 & -0.0041 & -0.0009 & -1.0078 \end{pmatrix}$$

Table 2: Typical Mueller matrix results for the SpectroLab sample at specular reflection half-angle of 15 degrees.
wavelength (nm): 600.0 Sample: SpectroLab Orientation: horizontal.

$$3.530 \times 10^{-2} \cdot \begin{pmatrix} 1.0000 & -0.0796 & -0.0006 & -0.0082 \\ -0.0811 & 1.0090 & 0.0052 & 0.0162 \\ 0.0170 & 0.0103 & -1.0049 & -0.0089 \\ -0.0165 & 0.0078 & 0.0030 & -0.9997 \end{pmatrix}$$

wavelength (nm): 600.0 Sample: SpectroLab Orientation: vertical.

$$3.481 \times 10^{-2} \cdot \begin{pmatrix} 1.0000 & -0.0749 & 0.0149 & -0.0087 \\ -0.0642 & 1.0081 & 0.0103 & 0.0098 \\ -0.0104 & 0.0068 & -1.0047 & 0.0006 \\ 0.0011 & 0.0054 & 0.0106 & -1.0052 \end{pmatrix}$$

taken at the specular reflection angle when the incident angle was 15° corresponding to a "phase" angle of 30° in the parlance of the astronomical community. The results in Table 1 for the mirror, assumed to be an isotropic surface, indicate the accuracy and reproducibility of the measurement process. Noting that $M_{00} = (\tau_{max} + \tau_{min})/2$ is the average reflectance in this case, the value indicates the amount of signal captured compared to the through-put of the calibration at this wavelength. Assuming that the mirror's reflectance was $\gtrsim$95% at these wavelengths, the M_{00} result above would be primarily indicative of the ratio in the effective aperture size between the calibration measurements (done in transmission) and the mirror measurements (done in reflection). Assuming the mirror is isotropic, all elements of the matrices of the two mirror orientations should be the same. Therefore, the differences, all within ±0.003, indicate the noise level of the measurement. The isotropic assumption also implies that the entries in the upper right and lower left 2×2 blocks should be zero and are therefore attributable to system bias and noise in the measurement process. These entries then indicate errors of about 0.01 as shown, or about 0.012 relative to the M_{00} matrix element.

Matrices for the SpectroLab solar cell fragment given in Table 2 indicate a level a reproducibility in the measurement with differences being $\lesssim$0.01 relative to the M_{00} element. However, in this case the average reflectance (M_{00}) is only about 4.4% of that of the mirror, and so the off-diagonal values represent a significant fraction of the overall polarization properties. The similar results of the measurements at the two orientations would seem to indicate that the sample is isotropic, and Eq. (10) may be valid even though the sample itself has a definite structural orientation due to the electrical contact strips (see Fig. 4). The two most significant off-diagonal entries are M_{01} and M_{10}, and this matrix is approximated by Eq. (10) when $\psi \approx -42.8^\circ$ and $\Delta \approx 0$, indicating a slight polarization dependence in the reflection coefficient whereas a similar calculation for the mirror yields $\psi \approx -45.3^\circ$ and $\Delta \approx 0$.

The average M_{00} element of the two orientations of the SpectroLab sample is shown in Fig. 6 normalized to the M_{00} element of the mirror at that wavelength. It shows no significant wavelength dependence over and above that of the mirror itself. The variation of the mirror reflectance with wavelength is probably due to systematic differences between mirror measurement and calibration measurements. Thus the mirror serves as a reference surface in this instance.

Fig. 7 depicts the wavelength dependence of all the Mueller matrix elements of the both the mirror and the Spectrolab sample. As noted above and in the Appendix, results at the shorter wavelengths are not as accurate as those between 600 and 700 nm because the nominal wavelength of the retarders of the generator is 670 nm. Nevertheless, the figure

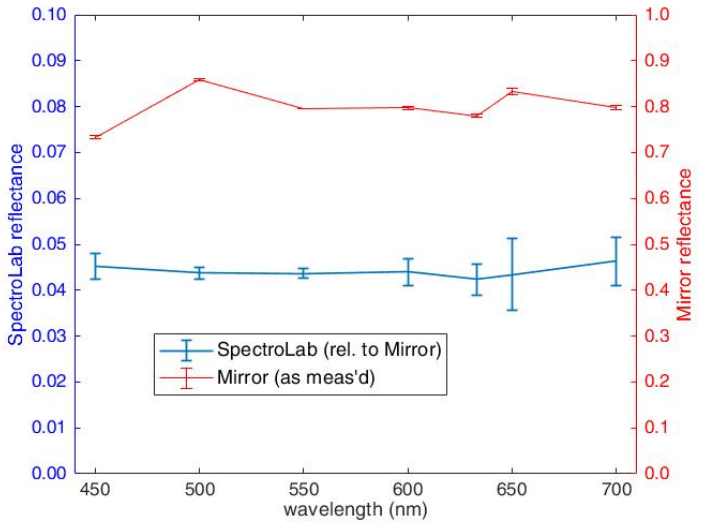

Fig. 6: The average specular reflectance of the SpectroLab solar cell fragment compared to that of the mirror and that of the mirror compared to the calibration throughput.

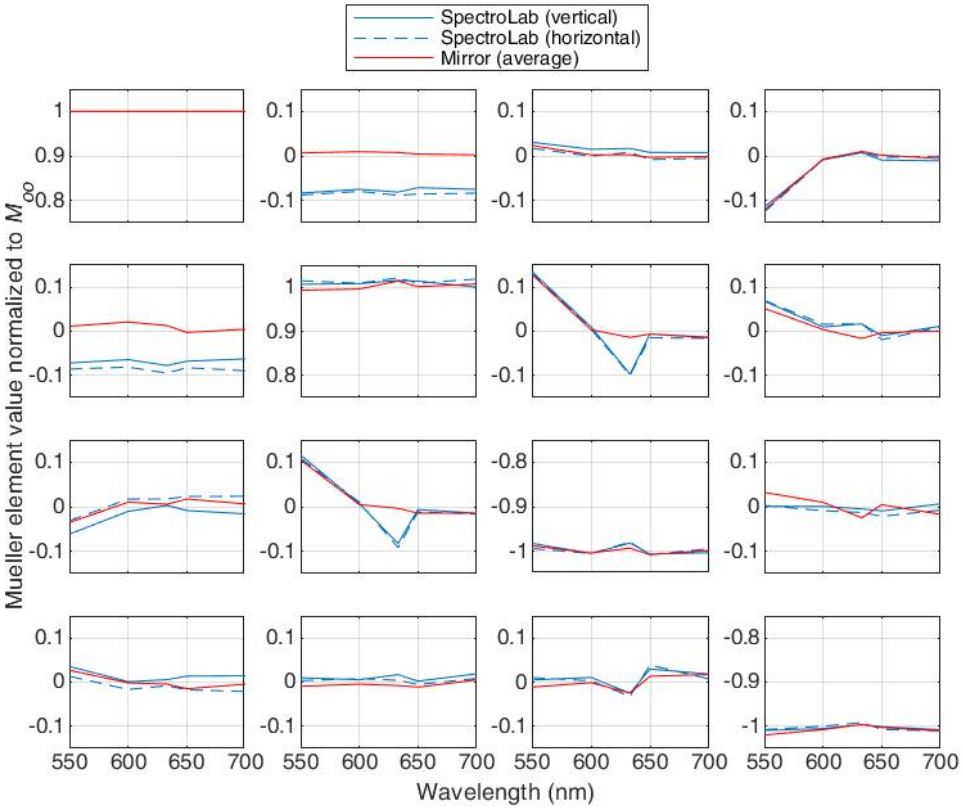

Fig. 7: The wavelength dependence of the Mueller matrix elements of the SpectroLab sample and the mirror relative to the respective M_{00} element ($\equiv \tau_{ave}$, Fig. 6). Data taken for specular reflection at a half angle of 15 degrees.

makes the deviations from the mirror results obvious in the M_{10} and M_{01} elements as well as an anomalous deviation at 633 nm for the M_{12} and M_{21} elements.

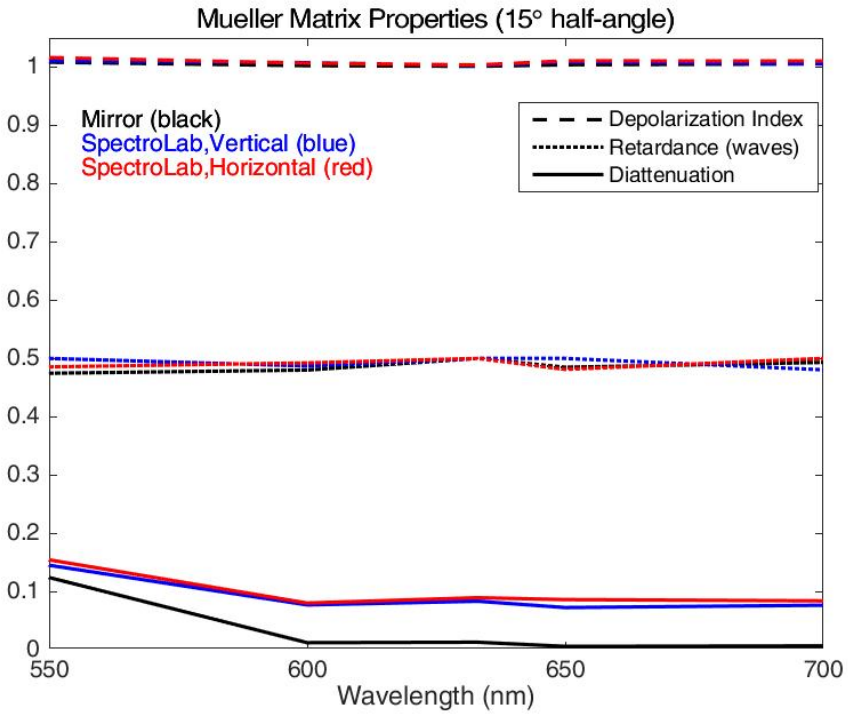

Fig. 8: The properties of the SpectroLab sample and the mirror as derived from Eqns. 7, 9, and 8 vs. wavelength

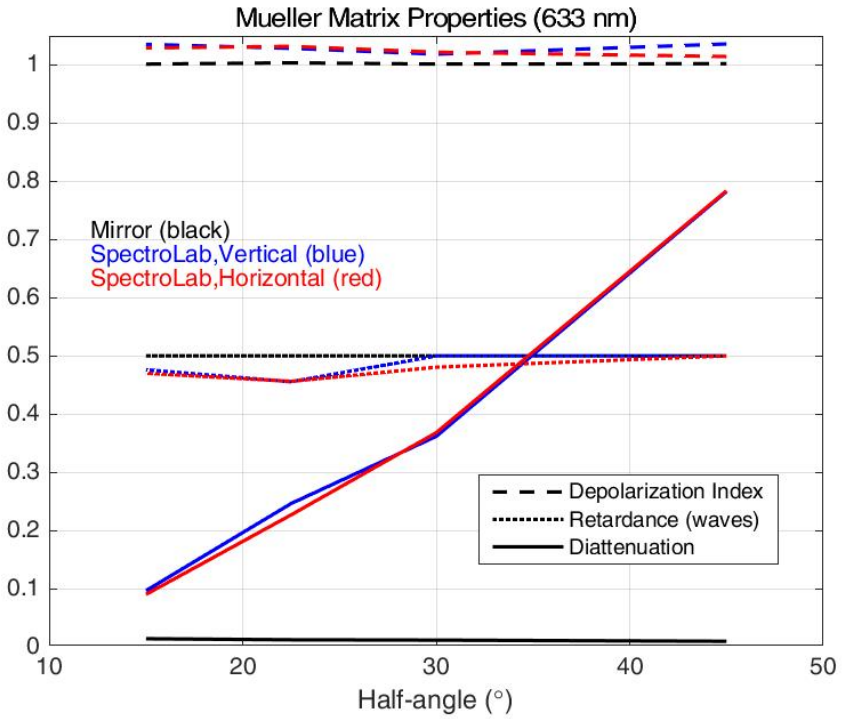

Fig. 9: The properties of the SpectroLab sample and the mirror as derived from Eqns. 7, 9, and 8 vs. scattering half-angle.

Fig. 8 and Fig. 9 depict the polarization index, diattenuation, and retardance of the mirror and sample that result from the application of Eqns. 7, 8, and 9. Note that calibration was in transmission and measurement was in reflection for this study and application of Eq. 9 does not explicitly take that into account. Hence retardation results of $\approx$ one-half wave indicate the phase change of 180° of the in-plane (horizontal) polarization component relative to the direction of propagation caused by reflection. These figures make clear that the major difference between the SpectroLab sample and the mirror is in the diattenuation parameter. This result is traceable to the differences in the M_{10} and M_{01} of the Mueller matrices. Since the diattenuation increases with angle, the cause is likely to be due to an anti-reflection coating that is over the photosensitive surface layer of the solar cell. Fig. 10 is a photo of a portion of a solar cell on which the coating is evident on a broken edge.

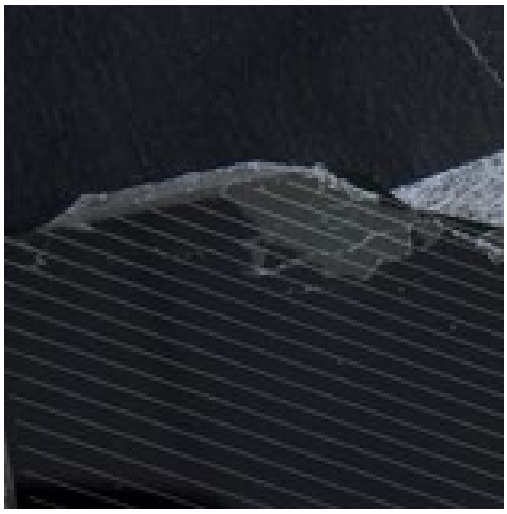

Fig. 10: A piece of a SpectroLab solar cell with the coating delaminated at a broken edge.

6. CONCLUSIONS AND FUTURE WORK

This study demonstrated the use of the Polarimetric Scatterometer of the Advanced Sensing Laboratory at the University of New South Wales - Canberra. The wavelength-resolved measurement of the Mueller matrix of a material of interest to the Space Situational Awareness community was described and results given. Work in progress will expand this study to other materials, a broader wavelength range, and a wider range of reflection angles. Those data could then be compared to observations of Earth-orbiting objects to determine the value of adding polarimetric data to spectroscopic or photometric data for material identification. noise.

7. ACKNOWLEDGEMENTS

The hardware for the original scatterometer was funded by AFOSR under a DURIP aware and the instrument was initially designed by Israel Vaughn. Work on the instrument has been funded by Asian Office of Aerospace R & D under award FA2386-15-1-4098

8. APPENDIX

Below is a listing of the generator's Stokes vectors (columns) as derived from the ECM for each wavelength attempted. "W00" refers to the S0 value of the first Stokes vector of each group (top left entry) and was used as the normalization constant for this listing. The value "evMin" refers to the minimum eigenvalue achieved by the ECM at that wavelength.

The wavelengths below 550 nm are notable in that they did not produce full modulations of the Stokes vector components and notably higher minimum eigenvalues. This was attributed to the wavelengths being too far from the design wavelengths of the generator retarders. The Mueller matrix elements for wavelengths 450 and 500 are not reported in Fig. 7, however those measurements were adequate for a reliable estimate of the average reflectance reported in Fig. 6.

wavelength:	450.0;	W00 =	-0.3365;	evMin =	2.0874e-01
1.0000	0.8817	0.9337	1.0303	0.8330	0.9447
0.8802	0.3744	0.1584	0.5828	-0.6288	-0.4273
0.1527	0.3519	-0.0027	-0.2401	0.2101	-0.4915
-0.1777	-0.5572	-0.7079	-0.5810	-0.0672	0.0196
wavelength:	500.0;	W00 =	-0.3719;	evMin =	8.8656e-02
1.0000	0.7150	0.7013	0.9312	0.7521	0.9745
0.7045	0.3060	-0.0089	0.3668	-0.4049	-0.2606
0.0212	0.4660	-0.1016	-0.5354	0.3418	-0.7596
0.1874	-0.3813	-0.6386	-0.2977	0.0462	-0.0366
wavelength:	550.0;	W00 =	-0.3058;	evMin =	1.0941e-02
1.0000	0.9385	0.9032	0.9729	0.9840	0.9395
0.9215	0.1367	-0.5827	0.2632	-0.4101	-0.2619
0.0317	0.8440	-0.0078	-0.7930	0.5700	-0.6730
0.0317	-0.4902	-0.6897	-0.4853	0.5621	-0.5464
wavelength:	600.0;	W00 =	-0.2881;	evMin =	2.1006e-04
1.0000	0.9962	1.0024	1.0104	1.0035	0.9997
0.9955	0.0351	-0.9174	0.0430	-0.2277	-0.1753
-0.0007	0.9660	-0.0066	-0.9559	0.3842	-0.4016
0.0177	-0.2843	-0.4176	-0.3103	0.8966	-0.8907
wavelength:	633.0;	W00 =	-0.2896;	evMin =	4.2063e-04
1.0000	0.9952	0.9990	1.0038	0.9948	1.0052
0.9855	0.0135	-0.9872	-0.0052	-0.1081	-0.0867
-0.0073	0.9917	0.0073	-0.9876	0.1854	-0.1865
0.0128	-0.1257	-0.1709	-0.1478	0.9669	-0.9651
wavelength:	650.0;	W00 =	-0.2880;	evMin =	3.0069e-04
1.0000	0.9990	1.0017	1.0049	1.0056	1.0028
0.9997	0.0066	-0.9979	-0.0045	-0.0483	-0.0358
-0.0122	0.9983	0.0056	-0.9993	0.0851	-0.0875
0.0073	-0.0625	-0.0948	-0.0885	0.9979	-1.0021
wavelength:	700.0;	W00 =	-0.2899;	evMin =	1.3127e-03
1.0000	0.9983	0.9986	0.9983	1.0010	0.9952
0.9914	0.0190	-0.9783	-0.0069	0.0990	0.1007
-0.0145	0.9924	0.0059	-0.9883	-0.1845	0.1780
-0.0010	0.1156	0.1673	0.1093	0.9683	-0.9676

9. REFERENCES

[1] Andrew D. Dianetti and John L. Crassidis. Space object material determination from polarized light curves. In *AIAA Scitech 2019 Forum*. AIAA, 2019-0377.

[2] J. Hostetler and H. Cowardin. Experimentally-derived bidirectional reflectance distribution function data in support of the orbital debris program office. In *Proceedings of the Advanced Maui Optical and Space Surveillance Technologies Conference*, 2019.

[3] Thomas Schildknecht, Esther Linder, Jiri Silha, Monika Hager, Nikolay Koshkin, Elen Korobeinikova, Seda Melikiants, Leonid Shakun, and Svetlana Strakhov. Photometric monitoring of non-resolved space debris and databases of optical light curves. In *Proceedings of the Advanced Maui Optical and Space Surveillance Technologies Conference*, 2015.

[4] A. Vananti, T. Schildknecht, and H. Krag. Reflectance spectroscopy characterization of space debris. *Advances in Space Research*, 59(10):2488–2500, 2017.

[5] Cone D. Reyes, J. Characterization of spacecraft materials using reflectance spectroscopy. In *Proceedings of the Advanced Maui Optical and Space Surveillance Technologies Conference*, 2018.

[6] Michael Bass, Casimer DeCusatis, Jay Enoch, Vasudevan Lakshminarayanan, Guifang Li, Carolyn Macdonald, Virendra Mahajan, and Eric Van Stryland. *Handbook of Optics, Third Edition*, volume Volume I: Geometrical and Physical Optics, Polarized Light, Components and Instruments. McGraw-Hill, Inc., 2009.

[7] Russell A. Chipman. *Handbook of Optics, Third Edition*, volume Volume I: Geometrical and Physical Optics, Polarized Light, Components and Instruments, book chapter 15: Polarimetry. McGraw-Hill, Inc., 2009.

[8] J. Scott Tyo, Dennis L. Goldstein, David B. Chenault, and Joseph A. Shaw. Review of passive imaging polarimetry for remote sensing applications. *Appl. Opt.*, 45(22):5453–5469, Aug 2006.

[9] Eric Compain, Stéphane Poirier, and Bernard Drevillon. General and self-consistent method for the calibration of polarization modulators, polarimeters, and mueller-matrix ellipsometers. *Applied Optics*, 38(16):3490–3502, 1999.

[10] C. Macias-Romero and P. Török. Eigenvalue calibration methods for polarimetry. *Journal of the European Optical Society - Rapid publications*, 7, 2012.

[11] Andrew Jolley, Greg Cohen, and Andrew Lambert. Use of neuromorphic sensors for satellite material characterisation. In *Imaging and Applied Optics 2019 (COSI, IS, MATH, pcAOP)*, OSA Technical Digest, page IM1B.4. Optical Society of America, 2019.

[12] José Jorge Gil and Eusebio Bernabeu. Depolarization and polarization indices of an optical system. *Optica Acta: International Journal of Optics*, 33(2):185–189, 1986.

[13] Shih-Yau Lu and Russell A. Chipman. Interpretation of mueller matrices based on polar decomposition. *J. Opt. Soc. Am. A*, 13(5):1106–1113, May 1996.

[14] R. M. A. Azzam and N. M. Bashara. *Ellipsometry and polarized light*. North-Holland Pub. Co. ; sole distributors for the U.S.A. and Canada, Elsevier North-Holland, Amsterdam ; New York : New York, 1977. Bibliographical references and indexes.